


RESEARCH

Open Access



Physical layer security analysis of IRS-based downlink and uplink NOMA networks

Si-Phu Le¹, Hong-Nhu Nguyen^{2*} , Nhat-Tien Nguyen², Cuu Ho Van², Anh-Tu Le¹ and Miroslav Voznak¹

*Correspondence:
nhu.nh@sgu.edu.vn

¹ Faculty of Electrical Engineering and Computer Science, VSB-Technical University of Ostrava, 17. Listopadu 2172/15, 70800 Ostrava, Czech Republic

² Faculty of Electronics and Telecommunications, Saigon University (SGU), Ho Chi Minh City, Vietnam

Abstract

In recent years, the development of intelligent reflecting surface (IRS) in wireless communications has enabled control of radio waves to reduce the detrimental impacts of natural wireless propagation. These can achieve significant spectrum and energy efficiency in wireless networks. Non-orthogonal multiple access (NOMA) technology, on the other hand, is predicted to improve the spectrum efficiency of fifth-generation and later wireless networks. Motivated by this reality, we consider the IRS-based NOMA network in the downlink and uplink scenario with a pernicious eavesdropper. Moreover, we investigated the physical layer security (PLS) of the proposed system by invoking the connection outage probability (COP), secrecy outage probability (SOP), and average secrecy rate (ASR) with analytical derivations. The simulation results reveal that (i) it is carried out to validate the analytical formulas, (ii) the number of meta-surfaces in IRS, transmit power at the base station, and power allocation parameters all play an essential role in improving the system performance, and (iii) it demonstrates the superiority of NOMA to the traditional orthogonal multiple access (OMA).

Keywords: Intelligent reflecting surface, Non-orthogonal multiple access, Physical layer security, Downlink, Uplink

1 Introduction

Future wireless networks are expected to play a pivotal role in society as they will offer access to intelligent applications such as autonomous driving and virtual and augmented reality. [1]. In order to offer ubiquitous services, though, wireless connectivity should be provided for everyone and everywhere [2]. Recently, intelligent reflecting surfaces (IRSs) have been proposed as one of the important technologies to realize wireless communication smart radio environment (SRE) systems [2]. A IRS is specifically made up of a number of small, inexpensive, almost passive reflecting elements (REs) that may be programmed and controlled by the network operator. Moreover, IRS can be modified to reflect and direct incoming signals in the desired directions [3–5]. Additionally, the terms reflecting intelligent surfaces (RISs) and large intelligent surfaces (LISs) are also used interchangeably for IRSs in [6]. The IRSs are known to have very significant spectrum efficiency (SE), as well as energy efficiency (EE) with a large number of passive REs in [7]. As a result of the IRS structure's simpler installation, it is now possible to deploy it more widely across the different urban infrastructures in both indoor and outdoor

settings, including factory roofs, street lights, and traffic signal poles as well as residential ceilings and rooftops. As a result, IRS is simple to integrate into the current wireless communication networks [8–10].

Furthermore, the increased demand for wireless access has prompted researchers to look beyond the traditional multiple access strategies in which users are multiplexed orthogonally according to time, frequency, or codes. The terms for multiplexing in time, frequency, and code are time division multiple access (TDMA), frequency division multiple access (FDMA), and code division multiple access (CDMA), respectively. Non-orthogonal multiple access (NOMA) has recently drawn a lot of interest and is now thought to be a strong contender for future wireless networks [11–14]. It is thought to support vast connectivity in addition to improving spectral efficiency when compared to orthogonal multiple access (OMA). It is possible to support more users than the number of accessible orthogonal resource blocks [15]. The main goal of NOMA is to enable non-orthogonal resource allocation among users in order to achieve multiple access (MA). The superposition coding (SC) technology, in which the signals of several users are multiplexed with varied power levels, served as an inspiration for NOMA in the power domain (PD)-NOMA. The overlaid messages are decoded at receivers using successive interference cancelation (SIC) [16]. Both downlink and uplink transmissions are compatible with NOMA. Users with poor channel conditions are typically given greater power for downlink NOMA so that their signals can be deciphered by treating other users' signals as noise. The base station must be able to identify signals from all users, which requires a well-designed power control mechanism for uplink NOMA [17].

In recent years, because both IRS and NOMA are extremely promising approaches, IRS was combined with NOMA in [18–21]. It has been demonstrated that combining IRS and NOMA allows for high data rate transfer while improving system performance. Furthermore, IRS-assisted NOMA improves spectrum resource usage. [22] proposed a simple concept for downlink transmission of IRS-assisted NOMA, in which the IRS is deployed to effectively serve the cell-edge user by aligning the reflected beam from the IRS. In [23], the authors proposed an energy-efficient approach for IRS-assisted NOMA, where the authors explore the tradeoff between the sum rate of NOMA users and total power usage. The authors of [24] provided various strategies to increase system performance for continuous phase shifts and discontinuous phase changes of IRS elements. [25] examined the downlink transmit power minimization problem for an IRS-powered NOMA network. The author in [26] investigated the performance of downlink and uplink IRS Networks. In [27], a IRS-assisted NOMA system was compared to a classic OMA system with/without IRS and a traditional NOMA system without IRS, and simulation results revealed that the IRS-assisted NOMA system outperformed the others in terms of rate performance.

Because electromagnetic transmission has the nature of broadcasting, which makes internet of thing (IoT) communication vulnerable to eavesdropping assaults, communication security, and secret protection are highly important in wireless communication networks [28, 29]. Traditional security approaches rely primarily on authentication and encryption, both of which are implemented at the upper layer of a wireless communication system but are generally independent of the physical layer. However, key management is problematic using classical encryption technologies [30]. From the standpoint

of information theory, physical layer security (PLS) technology exploits the indeterminacy and time-variability of the wireless channel to realize secure communication of encrypted links without a key [31] and has established a potential solution for secure wireless communication. In [32], beamforming was employed to decrease the system’s transmitted power under the limitation of secrecy rate. When the eavesdropper’s channel is superior to the user’s and both channels are highly correlated in space, joint beamforming was utilized to improve the user’s secrecy rate in [33]. In [34], the secrecy outage probability (SOP) was calculated in a IRS-aided wireless communication system and the effect of the number of reflectors in the IRS on secrecy performance was investigated. In [35], two techniques were described to improve the PLS of a IRS-aided multiple-input single-output (MIMO) system. In [36], a minimum-secrecy-rate maximization problem was solved to improve the overall system’s secrecy performance when the system has several legitimate users and multiple eavesdroppers. The author in [37] studied the PLS of a multi-user situation for an IRS-NOMA network, providing accurate and asymptotic SOPs. An IRS was used to aid a cell-edge user in [38], where the secrecy performance in the Nakagami- m fading channel was examined. In [39], the secrecy performance and diversity order are analyzed for the IRS-based NOMA network. The SOP and average secrecy capacity (ASC) are studied of IRS-based NOMA network under the Rayleigh fading channel in [40].

1.1 Motivation and contribution

According to the previous study, current IRS research priorities include generic IRS applications, the inherent integration of NOMA and IRS, and the PLS of IRS-aided wireless networks. The author in [40] investigated the PLS of IRS-aided NOMA for a downlink scenario under the Rayleigh fading channel. But the author does not consider for uplink scenario and the Nakagami- m fading channel for direct link. Therefore, to fill this gap, we analyzed the PLS of the IRS-aided NOMA network under the Nakagami- m fading channel for the downlink–uplink scenario. In addition, we have added Table 1 to compare the proposed work with the current literature. The detailed contributions of this study, in particular, can be summarized as follows:

- We considered the downlink–uplink IRS-based NOMA network, in which a base station (BS) sends and receives the signal from user 1 (D_1) and user 2 (D_2), IRS reflects and receives the signals from D_2 in the presence of an eavesdropper.

Table 1 A comparison of this work to related publications

	Our study	[32]	[33]	[34]	[35]	[36]	[39]	[40]
Secure downlink IRS-OMA	✓	✓	✓	✓	✓		✓	✓
Secure uplink IRS-OMA	✓							
Secure downlink IRS-NOMA	✓					✓	✓	✓
Secure uplink IRS-NOMA	✓							
All users use the Nakagami channel	✓							
COP Analysis	✓							
SOP Analysis	✓			✓			✓	✓
ASR Analysis	✓				✓	✓		✓

- We analyzed the PLS of the proposed system. Specifically, we provide the reliability and security analysis of the downlink–uplink by developing analytical formulas for the connection outage probability (COP), SOP, and ASR for the legitimate user D_1 , D_2 , an eavesdropper.
- We offer thorough simulations not only to validate the theoretical analysis results but also to provide some important technical insights. Throughout the numerical results, we emphasize the critical influence of utilizing the IRS. Following that, we demonstrate the effect of the number of IRS elements on the proposed system’s downlink–uplink.

1.2 Organization

The rest of this paper is structured as follows. Section 2 analyzes the system model of IRS-based NOMA networks with the downlink and uplink cases. Section 3 presents the channel model for the system. In Sect. 4, the downlink performance analysis is carried out, and in Section 5, the uplink performance analysis. Section 6 depicts a simulation of the model. Section 7 concludes the paper.

2 Method

2.1 System model

In Fig. 1, we consider the IRS-based downlink and uplink NOMA network, which consists of a BS, an IRS with N reflecting elements, and two receivers, D_1 and D_2 . The network is communicating while being intercepted by an eavesdropper (E). In more detail, D_1 is the near user that can be directly communicated with BS, but D_2 is the far user that requires an IRS’s assistance in order to communicate due to the long distance and obstructions. In addition, the reflection-coefficient matrix of IRS is denoted by $\Phi = \text{diag}(\alpha_1 e^{j\varphi_1}, \alpha_2 e^{j\varphi_2}, \dots, \alpha_N e^{j\varphi_N})$, ($j = \sqrt{-1}$), where $\alpha_n \in [0, 1]$ is the amplitude-reflection coefficient and $\varphi_n \in [0, 2\pi)$ is the phase-shift variable of the n th element that can be adjusted by the IRS with ($n = 1, 2, \dots, N$). Furthermore, we assume all wireless links following Nakagami- m fading. Particularly, $\mathbf{h}_1^d = [h_{1,1}^d, h_{1,2}^d, \dots, h_{1,N}^d]$, $\mathbf{h}_1^u = [h_{1,1}^u, h_{1,2}^u, \dots, h_{1,N}^u]^T$, $\mathbf{h}_2^d = [h_{2,1}^d, h_{2,2}^d, \dots, h_{2,N}^d]^T$ and $\mathbf{h}_2^u = [h_{2,1}^u, h_{2,2}^u, \dots, h_{2,N}^u]$ denotes the complex channel coefficient from BS-IRS, IRS-BS, IRS- D_2 , D_2 -IRS, respectively. Table 2 lists the primary parameters and functions.

2.2 Signal model of downlink

In this downlink section, the BS sends the superposed signal $s = \sqrt{\eta_1 P_{BS}} s_1^d + \sqrt{\eta_2 P_{BS}} s_2^d$ to D_i , in which, is the signal of D_i . Please take note that since user D_2 is assumed to be further away than the other user, a larger portion of power must be provided for user D_2 , i.e., condition $\eta_1 < \eta_2$ for user fairness and assume fixed power allocation splitting between two users [22]. The received signals at D_1 are given by

$$y_{D_1}^d = d_g^{-\frac{\beta}{2}} g_d s + \tau_1. \tag{1}$$

The corresponding signal-to-interference-plus-noise ratio (SINR) at D_1 to detect s_2^d is given by

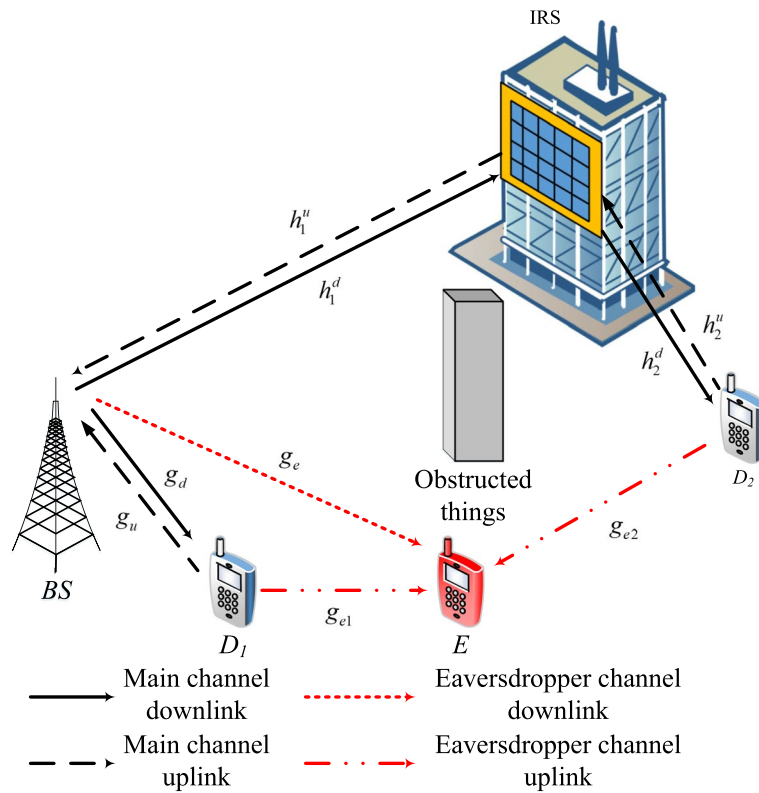


Fig. 1 The IRS downlink and uplink system model

$$\gamma_{D_1}^{d,2} = \frac{d_g^{-\beta} \eta_2 \psi |g_d|^2}{d_g^{-\beta} \eta_1 \psi |g_d|^2 + 1}, \tag{2}$$

where $\psi = \frac{P_{BS}}{N_0}$ denotes the transmit signal-to-noise ratio (SNR) of the BS.

After implementing the SIC, the corresponding SNR of D_1 when detecting the own signal is given by

$$\gamma_{D_1}^{d,1} = d_g^{-\beta} \eta_1 \psi |g_d|^2. \tag{3}$$

Next, the received signal at D_2 is given by

$$y_{D_2}^d = d_1^{-\frac{\beta}{2}} d_2^{-\frac{\beta}{2}} \mathbf{h}_1^d \Phi \mathbf{h}_2^d s + \tau_2. \tag{4}$$

The corresponding SINR of D_2 to detect the own signal is given by

$$\gamma_{D_2}^{d,2} = \frac{d_1^{-\beta} d_2^{-\beta} \eta_2 \psi |\mathbf{h}_1^d \Phi \mathbf{h}_2^d|^2}{d_1^{-\beta} d_2^{-\beta} \eta_1 \psi |\mathbf{h}_1^d \Phi \mathbf{h}_2^d|^2 + 1}. \tag{5}$$

At the E , the received signal can be expressed as

$$y_E^d = d_{g_e}^{-\frac{\beta}{2}} g_e s + \tau_e. \tag{6}$$

Table 2 Definitions for key parameter

Symbol	Description
$\text{diag}(x)$	Stands for a diagonal matrix for a vector x , where each diagonal element corresponds to an element in x
x^T	The transposition of x
$\mathbb{E}[\cdot]$	The expectation
$f_x(\cdot)$	The PDF of a random variable
$F_x(\cdot)$	The CDF of a random variable
$k!$	The factorial operation
$\text{Pr}(\cdot)$	The probability
$ \cdot $	The absolute operations
$I_a(\cdot)$	The modified Bessel function of the first kind
$Q_a(\cdot)$	The Marcum Q-function
$\Gamma(\cdot)$	The gamma function
$\gamma(\cdot, \cdot)$	The lower incomplete gamma function
s_i^d	The transmitted signals to $D_i, (i = 1, 2)$
s_i^u	The transmit signals of D_i
P_{BS}	The transmit power of BS
P_{D_i}	The transmit power of D_i
η_i	The power allocation coefficients with $(\eta_1 + \eta_2 = 1)$
β	The path loss exponent
τ_1	The additive white Gaussian noises (AWGN) at D_1 with zero mean and variance N_0
τ_2	The AWGN at D_2 with zero mean and variance N_0
τ_{BS}	The AWGN at BS
τ_e	The AWGN at E with the same variance N_e
R_i	The target data rate of users D_i
R_{Ei}	The secrecy rate of the user D_i
K	Accuracy-complexity tradeoff parameter
d_1	The distance from BS-IRS
d_2	The distance from IRS- D_2
d_g	The distance from BS- D_1
d_{ge}	The distance from BS- E
d_{ge1}	The distance from D_1 - E
d_{ge2}	The distance from D_2 - E
$h_{1,n}^d$	The channel coefficient from BS- n th reflecting element
$h_{1,n}^u$	The channel coefficient from n th reflecting element-BS
$h_{2,n}^d$	The channel coefficient from n th reflecting element- D_2
$h_{2,n}^u$	The channel coefficient from D_2 - n th reflecting element
g_d	The channel coefficient from BS- D_1
g_u	The channel coefficient from D_1 -BS
g_e	The channel coefficient from BS- E
g_{e1}	The channel coefficient from D_1 - E
g_{e2}	The channel coefficient from D_2 - E

In this work, like [41] and [42], parallel interference cancelation (PIC) is used at E to distinguish the superimposed mixture. Then, the corresponding SNR at E can be expressed as

$$\gamma_E^{d,i} = d_{ge}^{-\beta} \eta_i \psi_e |g_e|^2, \tag{7}$$

where $\psi_e = \frac{P_{BS}}{N_e}$.

2.3 Signal model of uplink

In the uplink section, the received signal at the BS is written by

$$y_{D_1}^u = d_g^{-\frac{\beta}{2}} g_u \sqrt{\eta_1 P_{D_1}} s_1^u + d_1^{-\frac{\beta}{2}} d_2^{-\frac{\beta}{2}} \mathbf{h}_1^u \Phi \mathbf{h}_2^u \sqrt{\eta_2 P_{D_2}} s_2^u + \tau_{bs}. \tag{8}$$

The corresponding SINR of BS, when decoded the signal of D_1 , is given by

$$\gamma_{D_1}^u = \frac{d_g^{-\beta} \eta_1 \psi_1 |g_u|^2}{d_1^{-\beta} d_2^{-\beta} \eta_2 \psi_2 |\mathbf{h}_1^u \Phi \mathbf{h}_2^u|^2 + 1}, \tag{9}$$

where $\psi_1 = \frac{P_{D_1}}{N_0}$, $\psi_2 = \frac{P_{D_2}}{N_0}$.

Following the completion of the SIC, the corresponding SNR to detect the signal of D_2 is given by

$$\gamma_{D_2}^u = d_1^{-\beta} d_2^{-\beta} \eta_2 \psi_2 |\mathbf{h}_1^u \Phi \mathbf{h}_2^u|^2. \tag{10}$$

The received signal at E can be expressed as

$$y_E^u = d_{ge1}^{-\frac{\beta}{2}} g_{e1} \sqrt{P_{D_1}} s_1^u + d_{ge2}^{-\frac{\beta}{2}} g_{e2} \sqrt{P_{D_2}} s_2^u + \tau_e. \tag{11}$$

Similar to (7), we can continue to apply PIC, then the SNR at E can be written by [41, 42]

$$\gamma_E^{u,i} = d_{gei}^{-\beta} \eta_i \psi_{ei} |g_{ei}|^2, \tag{12}$$

where $\psi_{ei} = \frac{P_{D_i}}{N_e}$, ($i = 1, 2$).

3 Channel model

Based on [43], the channel gain g_z follows Nakagami- m distribution with fading parameter m_{g_z} and $\mathbb{E}[|g_z|^2] = \lambda_{g_z}$ with $z = \{d, u, e, e1, e2\}$. Therefore, the probability density function (PDF) of $|g_z|^2$ is given by

$$f_{|g_z|^2}(x) = \frac{m_{g_z}^{m_{g_z}} x^{m_{g_z}-1}}{\lambda_{g_z}^{m_{g_z}} \Gamma(m_{g_z})} e^{-\frac{m_{g_z} x}{\lambda_{g_z}}}. \tag{13}$$

Next, the cumulative distribution function (CDF) is expressed as

$$\begin{aligned} F_{|g_z|^2}(x) &= 1 - \frac{1}{\Gamma(m_{g_z})} \Gamma\left(m_{g_z}, \frac{m_{g_z} x}{\lambda_{g_z}}\right) \\ &= 1 - e^{-\frac{m_{g_z} x}{\lambda_{g_z}}} \sum_{k=0}^{m_{g_z}-1} \frac{1}{k!} \left(\frac{m_{g_z} x}{\lambda_{g_z}}\right)^k, \end{aligned} \tag{14}$$

Next, we can rewrite the channel of D_2 as $|\mathbf{h}_1^v \Phi \mathbf{h}_2^v| = \left| \sum_{n=1}^N \alpha_n h_{1,n}^v h_{2,n}^v e^{j\varphi_n} \right|$ with $v = \{d, u\}$.

To obtain the best channel of $BS-IRS-D_2$, we adjust the phase-shift element of IRS to maximize $\left| \sum_{n=1}^N \alpha_n h_{1,n}^v h_{2,n}^v e^{j\varphi_n} \right|$. Next, by setting the optimal phase-shift φ_n , this implies that the phases of all $h_{1,n}^v h_{2,n}^v e^{j\varphi_n}$ can be set to be the same. Furthermore, the generalized solution can be obtained as $\varphi_n = \bar{\varphi} - \arg(h_{1,n}^v h_{2,n}^v)$, where $\bar{\varphi} \in [0, 2\pi)$ denotes the arbitrary constant. By applying the optimal phase-shift for φ_n , we can express as [26]

$$|\mathbf{h}_1^v \Phi \mathbf{h}_2^v|^2 = \alpha^2 \left| \sum_{n=1}^N h_{1,n}^v h_{2,n}^v \right|^2, \tag{15}$$

where $\alpha_n = \alpha, \forall n$. Denote $X_v = \frac{\left(\sum_{n=1}^N |h_{1,n}^v| |h_{2,n}^v| \right)^2}{2^{N(1-\omega_v)}}$, in which, $\lambda_v = \frac{N\omega_v}{1-\omega_v}$, $\omega_v = \frac{1}{m_{1,n}^v m_{2,n}^v} \left(\frac{\Gamma(m_{1,n}^v + 1/2)}{\Gamma(m_{1,n}^v)} \right)^2 \left(\frac{\Gamma(m_{2,n}^v + 1/2)}{\Gamma(m_{2,n}^v)} \right)^2$, where $m_{i,n}^v$ are denoted fading parameters of $h_{i,n}^v$. With N as a large number and applying the central limit theorem (CLT), X_v follows the noncentral chi-square distribution. Next, the PDF and CDF are given by [26]

$$\begin{aligned} f_{X_v}(x) &= \frac{\lambda_v^{1/4}}{2} e^{-\frac{x+\lambda_v}{2}} x^{-1/4} I_{-1/2}(\sqrt{\lambda_v x}) \\ &= e^{-\frac{x+\lambda_v}{2}} \sum_{j=0}^{\infty} \frac{\lambda_v^j x^{j-1/2}}{j! 2^{2j+1/2} \Gamma(j+1/2)}, \end{aligned} \tag{16}$$

and

$$\begin{aligned} F_{X_v}(x) &= 1 - Q_{1/2}(\sqrt{\lambda_v}, \sqrt{x}) \\ &= e^{-\frac{\lambda_v}{2}} \sum_{j=0}^{\infty} \frac{\lambda_v^j \gamma(j+1/2, x/2)}{j! 2^j \Gamma(j+1/2)}. \end{aligned} \tag{17}$$

4 Performance analysis for downlink

In this section, we derive the closed-form of COP, SOP, and ASR for user D_i with the downlink scenario.

4.1 COP analysis

4.1.1 COP OF D_1

The COP of user D_1 is defined as the probability of an interruption occurring in the connection of user D_1 when the connection of user D_2 is also interrupted. Therefore, the COP of user D_1 can be expressed by [44, 45]

$$COP_{D_1}^d = 1 - \Pr(\gamma_{D_1}^{d,2} > \gamma_{th2}, \gamma_{D_1}^{d,1} > \gamma_{th1}), \tag{18}$$

where $\gamma_{thi} = 2^{R_i} - 1$.

Proposition 1 *The closed-form expression for COP at D_1 is given by*

$$COP_{D_1}^d = 1 - e^{-\varepsilon} \sum_{k=0}^{m_{g_d}-1} \frac{\varepsilon^k}{k!}, \tag{19}$$

where $\varepsilon = \frac{m_{g_d} \rho}{\lambda_{g_d}}$, $\rho = \max \left(\frac{\gamma_{th2}}{(\eta_2 - \gamma_{th2} \eta_1) d_g^{-\beta} \psi}, \frac{\gamma_{th1}}{d_g^{-\beta} \eta_1 \psi} \right)$.

Proof From (18), $COP_{D_1}^d$ can be written as

$$\begin{aligned} COP_{D_1}^d &= 1 - \Pr \left(\frac{d_g^{-\beta} \eta_2 \psi |g_d|^2}{d_g^{-\beta} \eta_1 \psi |g_d|^2 + 1} > \gamma_{th2}, \right. \\ &\quad \left. d_g^{-\beta} \eta_1 \psi |g_d|^2 > \gamma_{th1} \right) \\ &= 1 - \Pr \left(|g_d|^2 > \frac{\gamma_{th2}}{(\eta_2 - \gamma_{th2} \eta_1) d_g^{-\beta} \psi}, \right. \\ &\quad \left. |g_d|^2 > \frac{\gamma_{th1}}{d_g^{-\beta} \eta_1 \psi} \right). \end{aligned} \tag{20}$$

We let $\rho = \max \left(\frac{\gamma_{th2}}{(\eta_2 - \gamma_{th2} \eta_1) d_d^{-\beta} \psi}, \frac{\gamma_{th1}}{d_d^{-\beta} \eta_1 \psi} \right)$, note that when we set power allocation coefficients, we need to ensure that $\eta_2 - \gamma_{th2} \eta_1 > 0$. Based on the CDF function of $|g_d|^2$ from (14), $COP_{D_1}^d$ can be derived as

$$COP_{D_1}^d = F_{|g_d|^2}(\rho) = 1 - e^{-\varepsilon} \sum_{k=0}^{m_{g_d}-1} \frac{\varepsilon^k}{k!}, \tag{21}$$

where $\varepsilon = \frac{m_{g_d} \rho}{\lambda_{g_d}}$. The proof is now complete. □

4.1.2 COP OF D_2

The COP of D_2 occurs when D_2 cannot detect correctly the own signal. So, the COP of D_2 can be defined by

$$COP_{D_2}^d = 1 - \Pr \left(\gamma_{D_2}^{d,2} > \gamma_{th2} \right). \tag{22}$$

Proposition 2 *The closed-form expression for COP at D_2 is given by*

$$COP_{D_2}^d = e^{-\frac{\lambda_d}{2}} \sum_{j=0}^{\infty} \frac{\lambda_d^j \gamma \left(j + 1/2, \frac{\gamma_{th2} N (1 - \omega_d)}{2(\eta_2 - \gamma_{th2} \eta_1) d_1^{-\beta} d_2^{-\beta} \psi \alpha^2} \right)}{j! 2^j \Gamma(j + 1/2)}. \tag{23}$$

Proof From (22), $COP_{D_2}^d$ can write as (24), as shown at the top of the next page.

$$\begin{aligned}
 COP_{D_2}^d &= 1 - \Pr \left(\frac{d_1^{-\beta} d_2^{-\beta} \eta_2 \psi \alpha^2 \frac{\left(\sum_{n=1}^N |h_{1,n}^d| |h_{2,n}^d|\right)^2}{N(1-\omega_d)}}{d_1^{-\beta} d_2^{-\beta} \eta_1 \psi \alpha^2 \frac{\left(\sum_{n=1}^N |h_{1,n}^d| |h_{2,n}^d|\right)^2}{N(1-\omega_d)} + 1} > \gamma_{th2} \right) \\
 &= 1 - \Pr \left(\left(\sum_{n=1}^N |h_{1,n}^d| |h_{2,n}^d|\right)^2 > \frac{\gamma_{th2} N(1-\omega_d)}{(\eta_2 - \gamma_{th2} \eta_1) d_1^{-\beta} d_2^{-\beta} \psi \alpha^2} \right).
 \end{aligned} \tag{24}$$

Similar to (20), note that when we set power allocation coefficients, we need to ensure that $\eta_2 - \gamma_{th2} \eta_1 > 0$. The CDF of $\left(\sum_{n=1}^N |h_{1,n}^d| |h_{2,n}^d|\right)^2$ is given by (17). $COP_{D_2}^d$ can be derived as

$$\begin{aligned}
 COP_{D_2}^d &= F \left(\sum_{n=1}^N |h_{1,n}^d| |h_{2,n}^d| \right)^2 \left(\frac{\gamma_{th2} N(1-\omega_d)}{(\eta_2 - \gamma_{th2} \eta_1) d_1^{-\beta} d_2^{-\beta} \psi \alpha^2} \right) \\
 &= e^{-\frac{\lambda_d}{2}} \sum_{j=0}^{\infty} \frac{\lambda_d^j \gamma \left(j + 1/2, \frac{\gamma_{th2} N(1-\omega_d)}{2(\eta_2 - \gamma_{th2} \eta_1) d_1^{-\beta} d_2^{-\beta} \psi \alpha^2} \right)}{j! 2^j \Gamma(j + 1/2)}.
 \end{aligned} \tag{25}$$

The proof is now finished. □

4.2 SOP analysis

Assume the eavesdropper could decode sensitive information from *BS* by using multi-user detection techniques. Based on (7) and (14), the closed-form of user D_i can be given by [44]

$$\begin{aligned}
 SOP_{D_i}^d &= \Pr \left(\gamma_E^{d,i} > \xi_i \right) = \Pr \left(|g_e|^2 > \frac{\xi_i}{d_{ge}^{-\beta} \eta_i \psi_e} \right) \\
 &= 1 - F_{|g_e|^2} \left(\frac{\xi_i}{d_{ge}^{-\beta} \eta_i \psi_e} \right) = e^{-\mu_i} \sum_{k=0}^{m_{ge}-1} \frac{(\mu_i)^k}{k!},
 \end{aligned} \tag{26}$$

where $\mu_i = \frac{m_{ge} \xi_i}{d_{ge}^{-\beta} \eta_i \psi_e \lambda_{ge}}$, $\xi_i = 2^{R_i - R_{Ei}} - 1$.

4.3 ASR analysis

4.3.1 ASR OF D_1

The ASR of D_1 can be expressed as [46]

$$\begin{aligned}
 \bar{C}_{D_1}^d &= \mathbb{E} \left[\log_2 \left(\frac{1 + \gamma_{D_1}^{d,1}}{1 + \gamma_E^{d,1}} \right) \right]^+ \\
 &= \underbrace{\mathbb{E} \left[\log_2 \left(1 + \gamma_{D_1}^{d,1} \right) \right]}_{Z_1^d} - \underbrace{\mathbb{E} \left[\log_2 \left(1 + \gamma_E^{d,1} \right) \right]}_{Z_2^d},
 \end{aligned} \tag{27}$$

where $[X]^+ = \max\{0, X\}$ is to ensure the secrecy capacity strictly positive.

Proposition 3 The closed-form expression for ASR at D_1 is given by

$$\bar{C}_{D_1}^d = \frac{1}{\ln 2} \left[\frac{1}{\Gamma(m_{gd})} G_{2,3}^{3,1} \left(0, 1 \mid \frac{m_{gd}}{d_g^{-\beta} \eta_1 \psi \lambda_{gd}} \right) - \frac{1}{\Gamma(m_{ge})} G_{2,3}^{3,1} \left(0, 1 \mid \frac{m_{ge}}{d_{ge}^{-\beta} \eta_1 \psi_e \lambda_{ge}} \right) \right]. \tag{28}$$

Proof The details are given in Appendix A. □

4.3.2 ASR OF D_2

The ASR of D_2 can be expressed as [46]

$$\begin{aligned} \bar{C}_{D_2}^d &= \mathbb{E} \left[\log_2 \left(\frac{1 + \gamma_{D_2}^{d,2}}{1 + \gamma_E^{d,2}} \right) \right]^+ \\ &= \underbrace{\mathbb{E} \left[\log_2 \left(1 + \gamma_{D_2}^{d,2} \right) \right]}_{W_1^d} - \underbrace{\mathbb{E} \left[\log_2 \left(1 + \gamma_E^{d,2} \right) \right]}_{W_2^d}. \end{aligned} \tag{29}$$

Proposition 4 The closed-form expression for ASR at D_2 is given by (30), as shown at the top of the next page, where $\Theta = \frac{\eta_2 t_k + \eta_2}{2\eta_1}$, $t_k = \cos \left[\frac{(2k-1)\pi}{2K} \right]$.

$$\bar{C}_{D_2}^d = \frac{1}{\ln 2} \left[\frac{\pi \eta_2}{2\eta_1 K} e^{-\frac{j}{2}} \sum_{j=0}^{\infty} \sum_{k=1}^K \sqrt{1-t_k^2} \frac{\lambda_d^j \Gamma(j+1/2, \frac{\Theta N(1-t_k)}{2(\eta_2 - \Theta \eta_1) d_1^{-\beta} d_2^{-\beta} \psi \alpha^2})}{j! 2^j \Gamma(j+1/2)(1+\Theta)} - \frac{1}{\Gamma(m_{ge})} G_{2,3}^{3,1} \left(0, 1 \mid \frac{m_{ge}}{d_{ge}^{-\beta} \eta_2 \psi_e \lambda_{ge}} \right) \right]. \tag{30}$$

Proof The details are given in Appendix B. □

5 Performance analysis for uplink

In this section, we derive the closed-form of COP, SOP, and ASR for user D_i with the uplink scenario.

5.1 COP analysis

5.1.1 COPOF D_1

If D_1 is unable to accurately identify its own signal, the COP of D_1 will occur. As a result, the COP for the uplink of D_1 can be described as [26]

$$COP_{D_1}^u = 1 - \Pr(\gamma_{D_1}^u > \gamma_{th1}). \tag{31}$$

Proposition 5 The closed-form expression for COP at D_1 is given by

$$\begin{aligned}
 COP_{D_1}^u &= 1 - e^{-\frac{m_{gu}\theta_1}{\lambda_{gu}} - \frac{\lambda_u}{2}} \sum_{k=0}^{m_{gu}-1} \sum_{j=0}^{\infty} \sum_{q=0}^k \binom{k}{q} \left(\frac{1}{\theta_2}\right)^{k-q} \\
 &\quad \times \frac{\delta^k \lambda_u^j \Gamma(j+q+1/2)}{k!j!2^{2j+1/2}\Gamma(j+1/2)} \left(\delta + \frac{1}{2}\right)^{-(j+q+1/2)},
 \end{aligned} \tag{32}$$

where $\delta = \frac{m_{gu}\theta_1\theta_2}{\lambda_{gu}}$, $\theta_1 = \frac{\gamma_{th1}}{d_g^{-\beta}\eta_1\psi_1}$, $\theta_2 = \frac{d_1^{-\beta}d_2^{-\beta}\eta_2\psi_2\alpha^2}{N(1-\omega_u)}$.

Proof The details are given in Appendix C. □

5.1.2 COP OF D_2

Similarly to (31), when D_2 is unable to appropriately identify its own signal, the COP of D_2 happens. Consequently, the COP of D_2 can be described as follows:

$$\begin{aligned}
 COP_{D_2}^u &= 1 - \Pr(\gamma_{D_2}^u > \gamma_{th2}) \\
 &= 1 - \Pr\left(\theta_2 \left(\sum_{n=1}^N |h_{1,n}^u| |h_{2,n}^u|\right)^2 > \gamma_{th2}\right) \\
 &= 1 - \Pr\left(\left(\sum_{n=1}^N |h_{1,n}^u| |h_{2,n}^u|\right)^2 > \frac{\gamma_{th2}}{\theta_2}\right) \\
 &= F\left(\sum_{n=1}^N |h_{1,n}^u| |h_{2,n}^u|\right)^2 \left(\frac{\gamma_{th2}}{\theta_2}\right) \\
 &= e^{-\frac{\lambda_u}{2}} \sum_{j=0}^{\infty} \frac{\lambda_u^j \gamma(j+1/2, \frac{\gamma_{th2}}{2\theta_2})}{j!2^j \Gamma(j+1/2)}.
 \end{aligned} \tag{33}$$

5.2 SOP analysis

The SOP of user D_i can be given by

$$\begin{aligned}
 SOP_{D_i}^u &= \Pr(\gamma_E^{u,i} > \xi_i) \\
 &= \Pr\left(|g_{ei}|^2 > \frac{\xi_i}{d_{gei}^{-\beta}\eta_i\psi_{ei}}\right) \\
 &= 1 - F_{|g_{ei}|^2} \left(\frac{\xi_i}{d_{gei}^{-\beta}\eta_i\psi_{ei}}\right) \\
 &= e^{-\chi_i} \sum_{k=0}^{m_{gei}-1} \frac{(\chi_i)^k}{k!},
 \end{aligned} \tag{34}$$

where $\chi_i = \frac{m_{gei}\xi_i}{d_{gei}^{-\beta}\eta_i\psi_{ei}\lambda_{gei}}$.

5.3 ASR analysis

5.3.1 ASR OF D_1

The ASR of D_1 can be expressed as

$$\begin{aligned} \bar{C}_{D_1}^u &= \mathbb{E} \left[\log_2 \left(\frac{1 + \gamma_{D_1}^u}{1 + \gamma_E^{u,1}} \right) \right]^+ \\ &= \underbrace{\mathbb{E} [\log_2(1 + \gamma_{D_1}^u)]}_{Z_1^u} - \underbrace{\mathbb{E} [\log_2(1 + \gamma_E^{u,1})]}_{Z_2^u}. \end{aligned} \tag{35}$$

Proposition 6 The closed-form expression for ASR at D_1 is given by (36), as shown at the top of the next page, where $\phi = \frac{m_{gu}}{d_g^{-\beta} \eta_1 \psi_1 \lambda_{gu}}$.

$$\begin{aligned} \bar{C}_{D_1}^u &= \frac{1}{\ln(2)} e^{-\frac{\lambda_u}{2}} \sum_{k=0}^{m_{gu}-1} \sum_{j=0}^{\infty} \sum_{q=0}^k \binom{k}{q} \left(\frac{1}{\theta_2}\right)^{k-q} \left(\frac{1}{2}\right)^{-(j+q+1/2)} \frac{(\phi \theta_2)^k \lambda_u^j \phi^{-k-1}}{k! j! 2^{2j+1/2} \Gamma(j+1/2)} \\ &\quad \times H_{1,0:1,1:1,1}^{0,1:1,1:1,1} \left(\begin{matrix} (-k, 1, 1) & & (0, 1) \\ & - & (0, 1) \end{matrix} \middle| \begin{matrix} (1 - (j + q + 1/2), 1) \\ (0, 1) \end{matrix} \middle| \frac{1}{\phi}, 2\theta_2 \right) \\ &\quad - \frac{1}{\Gamma(m_{ge1}) \ln(2)} G_{2,3}^{3,1} \left(\begin{matrix} 0, 1 \\ 0, m_{ge1}, 0 \end{matrix} \middle| \frac{m_{ge1}}{d_{ge1}^{-\beta} \eta_1 \psi_{e1} \lambda_{ge1}} \right). \end{aligned} \tag{36}$$

□

Proof The details are given in Appendix D. □

5.3.2 ASR OF D_2

The ASR of D_2 can be expressed as

$$\begin{aligned} \bar{C}_{D_2}^u &= \mathbb{E} \left[\log_2 \left(\frac{1 + \gamma_{D_2}^u}{1 + \gamma_E^{u,2}} \right) \right]^+ \\ &= \underbrace{\mathbb{E} [\log_2(1 + \gamma_{D_2}^u)]}_{W_1^u} - \underbrace{\mathbb{E} [\log_2(1 + \gamma_E^{u,2})]}_{W_2^u}. \end{aligned} \tag{37}$$

Proposition 7 The closed-form expression for ASR at D_2 is given by

$$\begin{aligned} \bar{C}_{D_2}^u &= \frac{1}{\ln 2} e^{-\frac{\lambda_u}{2}} \sum_{j=0}^{\infty} \frac{\lambda_u^j}{j! 2^j \Gamma(j+1/2)} \\ &\quad \times G_{2,3}^{3,1} \left(\begin{matrix} 0, 1 \\ 0, 0, j+1/2 \end{matrix} \middle| \frac{1}{2\theta_2} \right) \\ &\quad - \frac{1}{\Gamma(m_{ge2}) \ln(2)} G_{2,3}^{3,1} \left(\begin{matrix} 0, 1 \\ 0, m_{ge2}, 0 \end{matrix} \middle| \frac{m_{ge2}}{d_{ge2}^{-\beta} \eta_2 \psi_{e2} \lambda_{ge2}} \right). \end{aligned} \tag{38}$$

Proof The details are given in Appendix E. □

6 Simulation results and discussion

In this section, we define sim. and ana. as short for simulation and analytical. Next, we verify our theoretical analysis by using Monte-Carlo simulation.

In Fig. 2, we plot the COP for downlink versus ψ (dB) with varying the number of elements. First, it can be easily observed that the COP curve corresponds exactly to the Monte Carlo simulation results. The simulation points of D_1 and D_2 correspond well to the analytical results obtained from (19) and (22), respectively. Furthermore, when the ψ rises, so will the system COP's performance. In terms of comparing the COPs of D_1 and D_2 , the simulation results show that user D_2 has the best scenario because it is assisted by IRS. In addition, the power allocation has a great impact on the COP performance. In addition, NOMA outperforms OMA for two users D_1 and D_2 in all SNR ranges.

Figure 3 illustrates the COP for downlink versus ψ (dB) with varying the number of elements N , we can see that the COP performance is improved by increasing the number of reflecting meta-surface elements N for D_2 . We can observe that the user D_2 supported by IRS has better COP performance than the unsupported user D_1 . The research gap between two users D_1 and D_2 increases when N is large. Moreover, in the case without IRS, we can observe the COP performance of D_1 is better than D_2 . This can be explained because the distance from BS to D_2 is larger than D_1 . In Fig. 4, the impacts of the SOP for the downlink of D_1 and D_2 versus the transmit power ψ_E (dB) with varying the target data rate of two users. We can see that the SOP increases significantly with increasing ψ_E (dB). Under the intended parameters, the suggested NOMA method has somewhat lower secrecy outage performance than OMA in high transmission power locations.

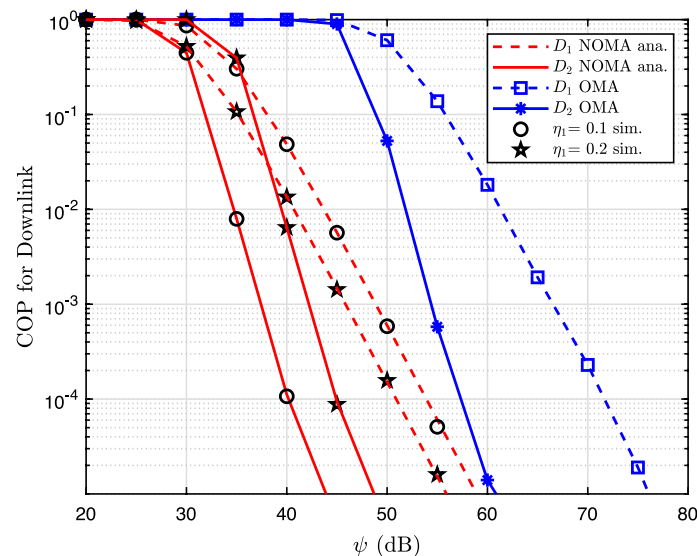


Fig. 2 COP for NOMA downlink system and OMA downlink system versus ψ as changing η_1 ($R_1 = 3$ (bps/Hz), $R_2 = 2$ (bps/Hz), $\beta = 2$, $d_g = 5$ (m), $d_1 = 10$ (m), $d_2 = 5$ (m), $m_{g_d} = m_{1,n}^d = m_{2,n}^d = 2$, $\lambda_{g_d} = 1$, $N = 8$, $\varphi = 0.9$)

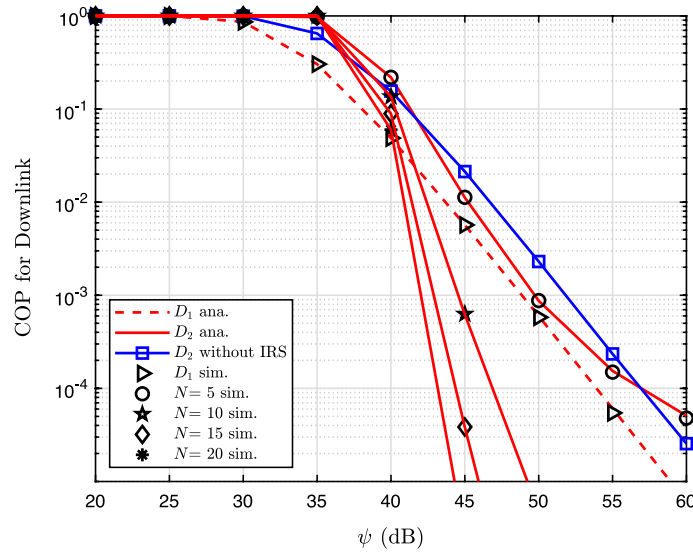


Fig. 3 COP for downlink system versus ψ as changing N ($\eta_1 = 0.1, R_1 = R_2 = 3$ (bps/Hz), $\beta = 2, d_g = 5$ (m), $d_1 = 10$ (m), $d_2 = 5$ (m), $m_{g_d} = m_{1,n}^d = m_{2,n}^d = 2, \lambda_{g_d} = 1, \varphi = 0.9$)

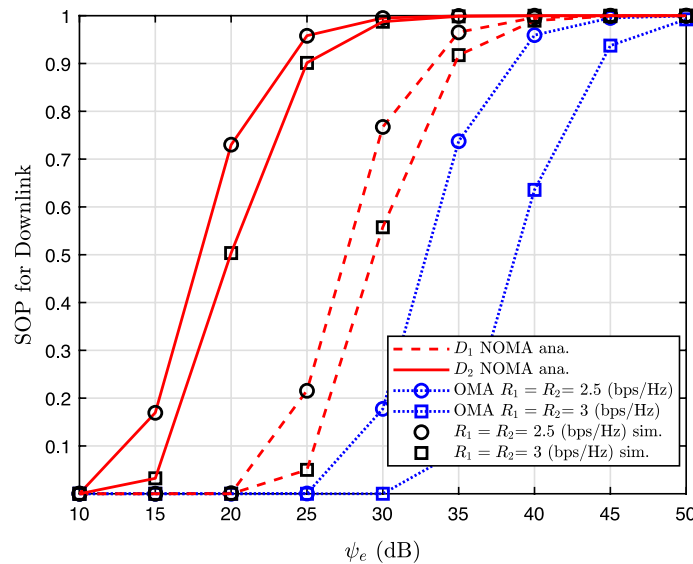


Fig. 4 SOP for NOMA downlink system and OMA downlink system versus ψ_e as changing $R_1 = R_2$ ($\eta_1 = 0.1, R_{E1} = R_{E2} = 1$ (bps/Hz), $\beta = 2, d_{g_e} = 5$ (m), $m_{g_e} = 2, \lambda_{g_e} = 1$)

Figure 5 depicts the ASR for downlink versus ψ (dB) varying the path loss β , assumed to be $K=100$ for the accuracy-complexity tradeoff parameter. First, it is obvious that ASR increases with transmit power ψ (dB). Second, the variation of β will change the ASR of two users D_i . It means the ASR is decreased when β is increased. Finally, for D_2 , when ψ (dB) is large enough, ASR of D_2 will converge at one point.

In Fig. 6, it plots the COP for uplink versus $\psi_1 = \psi_2$ (dB) with varying the number of elements N . It is discovered that the simulation points of D_1 and D_2 correspond well to

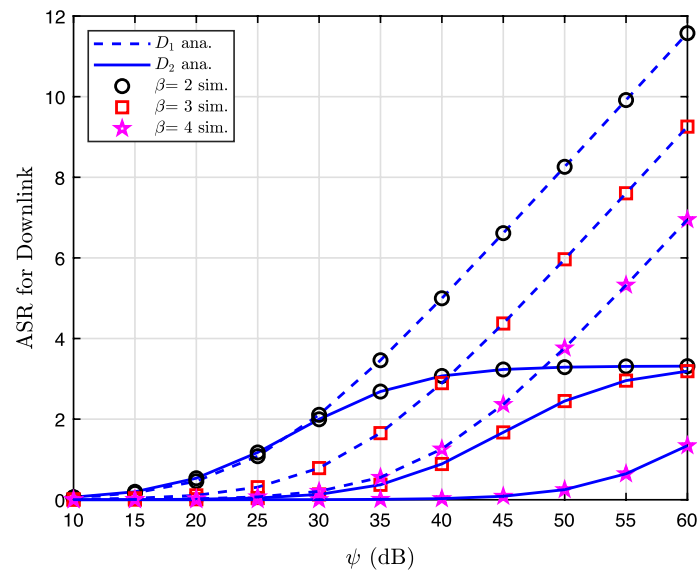


Fig. 5 ASR for downlink system versus ψ as changing β ($\eta_1 = 0.1, \beta = 2, d_g = 5$ (m), $d_1 = 10$ (m), $d_2 = 5$ (m), $d_{g_e} = 5$ (m), $\psi_e = -10$ (dB), $m_{g_d} = m_{1,n}^d = m_{2,n}^d = m_{g_e} = 2, \lambda_{g_d} = \lambda_{g_e} = 1, N = 8, \varphi = 0.9, K = 100$)

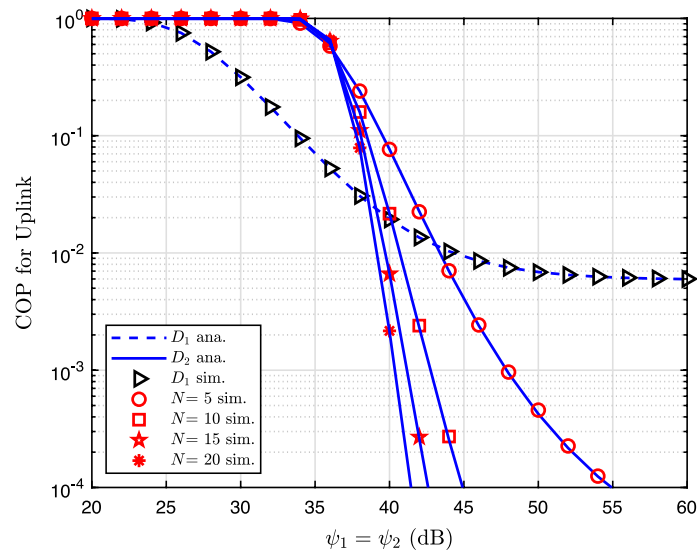


Fig. 6 COP for uplink system versus $\psi_1 = \psi_2$ as changing N ($\eta_1 = 0.1, R_1 = 0.5$ (bps/Hz), $R_2 = 0.5$ (bps/Hz), $\beta = 3, d_g = 5$ (m), $d_1 = 10$ (m), $d_2 = 5$ (m), $m_{g_d} = m_{1,n}^d = m_{2,n}^d = 2, \lambda_{g_d} = 1, \varphi = 0.9$)

the analytical results obtained from (30) and (31), respectively. Then, we can observe that when the transmit $\psi_1 = \psi_2$ (dB) increases, the COP of D_1 decreases and approaches a floor. Because of the uplink NOMA principle, D_2 's signal is viewed as interference when decoding D_1 's signal. Furthermore, when N increase, the performance COP of D_2 is improve significantly.

Figure 7 shows the COP for the uplink of two users D_1 and D with different fading values $m = 1$ and $m = 2$. It is apparent that $m = 2$ leads to a better channel, which is significant in improving the performance of destinations. The fundamental reason for this is

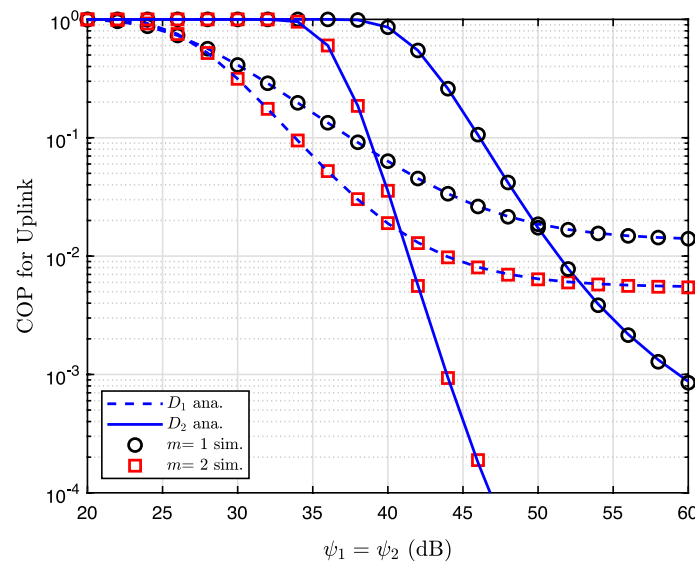


Fig. 7 COP for uplink system versus $\psi_1 = \psi_2$ as changing $m = m_{g_d} = m_{1,n}^d = m_{2,n}^d$ ($\eta_1 = 0.1, R_1 = 0.5$ (bps/Hz), $R_2 = 0.5$ (bps/Hz), $\beta = 2, d_g = 5$ (m), $d_1 = 10$ (m), $d_2 = 5$ (m), $\lambda_{g_d} = 1, N = 8, \varphi = 0.9$)

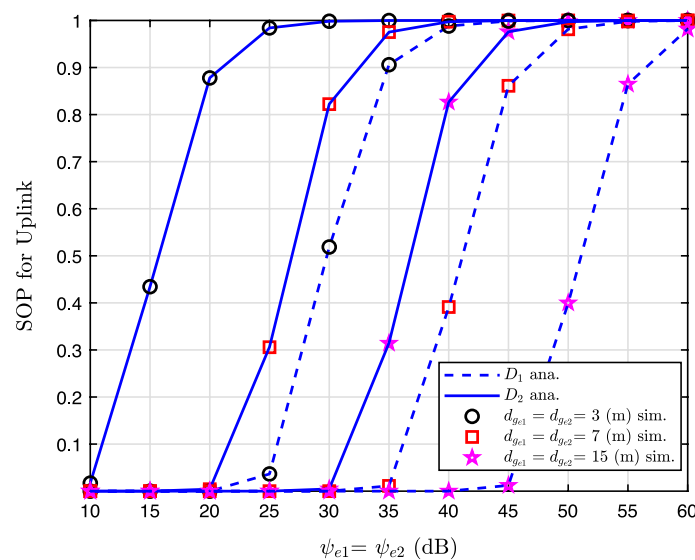


Fig. 8 SOP for uplink system versus $\psi_{e1} = \psi_{e2}$ as changing $d_{g_{e1}} = d_{g_{e2}}$ ($\eta_1 = 0.1, R_1 = 3$ (bps/Hz), $R_{E1} = R_{E2} = 1$ (bps/Hz), $R_2 = 2$ (bps/Hz), $\beta = 3, m_{g_{e1}} = m_{g_{e2}} = 2, \lambda_{g_{e1}} = \lambda_{g_{e2}} = 1$)

those principal SINR and SNR expressions depend on channel gains. As a result, larger channel gains result in higher SINR and SNR, and outage performance can be improved.

Figure 8 shows the SOP for the uplink of two users D_1 and D_2 with different distances from D_1 and D_2 to E . We can see that the wider the distance between two users and E , the secrecy performance of the two users is better. This is because, as the distance increases, the power allocated to user D_2 expands to meet its quality of service (QoS) requirements. As a

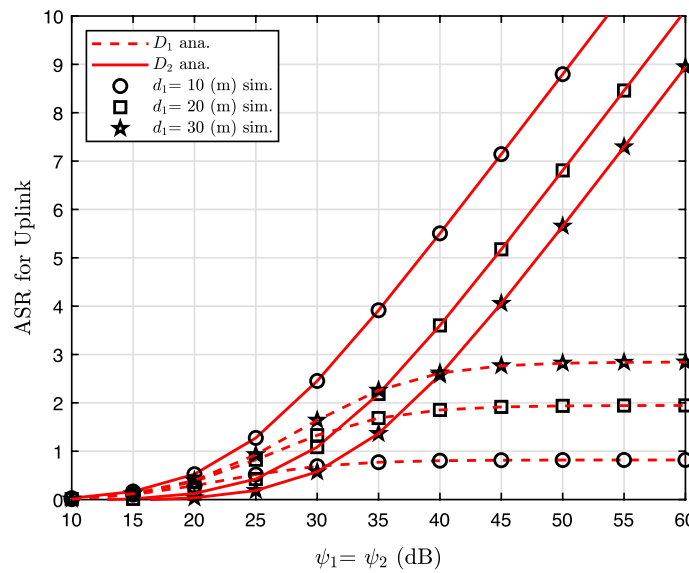


Fig. 9 ASR for uplink system versus $\psi_1 = \psi_2$ as changing d_1 ($\eta_1 = 0.1, \beta = 2, d_g = 5$ (m), $d_2 = 5$ (m), $d_{ge} = 5$ (m), $d_{ge1} = d_{ge2} = 1$ (m), $m_{gd} = m_{1,n}^d = m_{2,n}^d = 2, m_{ge1} = m_{ge2} = 3, \lambda_{gd} = \lambda_{ge} = \lambda_{ge1} = \lambda_{ge2} = 1, N = 8, \rho = 0.9$)

result, the power assigned to user D_1 will drop. Given a secrecy guard distance, two users perform better at a small distance than a large distance. In Fig. 9, the ASR curves for the uplink network of two users D_1 and D_2 are depicted. We observe that the simulated findings match the relevant analytical results obtained from (34) and (36). Then, we see that the ASR of user D_2 also converges to a ceiling. Moreover, the distance d_1 is large, which leads to a decrease in the ASR.

7 Conclusion

In this paper, we analyzed the secrecy performance for IRS-based downlink and uplink NOMA networks. Based on the proposed system, the closed-form of COP, SOP, and ASR are derived. All analytical results are verified by Monte Carlo simulations. We show numerical results for various secure performances under the influence of several parameters such as transmit SNR at the base station and the number of reflecting elements of IRS setup. In addition, the proposed IRS-based NOMA scheme is compared with OMA. The number of reflecting elements at the IRS and SNR level at the base station, as the major finding, contribute primarily to the improvement of security for IRS-aided NOMA systems.

Appendix A

From (27), Z_1^d can be written by

$$Z_1^d = \frac{1}{\ln 2} \int_0^\infty \frac{1 - F_{\gamma_{D_1}^{d,1}}(x)}{1 + x} dx. \tag{39}$$

Next, the formula for $F_{\gamma_{D_1}^{d,1}}(x)$ is as follows

$$\begin{aligned}
 F_{\gamma_{D_1}^{d,1}}(x) &= 1 - \Pr\left(|g_d|^2 > \frac{x}{d_g^{-\beta} \eta_1 \psi}\right) \\
 &= F_{|g_d|^2}\left(\frac{x}{d_g^{-\beta} \eta_1 \psi}\right) \\
 &= 1 - \frac{1}{\Gamma(m_{g_d})} \Gamma\left(m_{g_d}, \frac{m_{g_d} x}{d_g^{-\beta} \eta_1 \psi \lambda_{g_d}}\right).
 \end{aligned}
 \tag{40}$$

From (40) into (39), Z_1^d can be given by

$$\begin{aligned}
 Z_1^d &= \frac{1}{\Gamma(m_{g_d}) \ln(2)} \int_0^\infty \frac{\Gamma\left(m_{g_d}, \frac{m_{g_d} x}{d_g^{-\beta} \eta_1 \psi \lambda_{g_d}}\right)}{1+x} dx \\
 &= \frac{1}{\Gamma(m_{g_d}) \ln(2)} \\
 &\quad \times \int_0^\infty (x+1)^{-1} G_{1,2}^{2,0}\left(1 \mid m_{g_d}, 0 \mid \frac{m_{g_d} x}{d_g^{-\beta} \eta_1 \psi \lambda_{g_d}}\right) dx,
 \end{aligned}
 \tag{41}$$

where the Meijer G-function is $G_{p,1}^{m,n}(\cdot)$ [47, Eq. (9.301)]. Moreover, we employ the equalities [48, Eq. (2.6)] as

$$\Gamma(A, Bx) = G_{1,2}^{2,0}\left(1 \mid A, 0 \mid Bx\right).
 \tag{42}$$

With the extra help of [47, Eq. (7.811.5)], Z_1^d can be written by

$$Z_1^d = \frac{1}{\Gamma(m_{g_d}) \ln(2)} G_{2,3}^{3,1}\left(0, 1 \mid 0, m_{g_d}, 0 \mid \frac{m_{g_d}}{d_g^{-\beta} \eta_1 \psi \lambda_{g_d}}\right).
 \tag{43}$$

From (27), Z_2^d can be written by

$$Z_2^d = \frac{1}{\ln 2} \int_0^\infty \frac{1 - F_{\gamma_E^{d,1}}(x)}{1+x} dx.
 \tag{44}$$

According to (14), $F_{\gamma_E^{d,1}}(x)$ can be given by

$$F_{\gamma_E^{d,1}}(x) = 1 - \frac{1}{\Gamma(m_{g_e})} \Gamma\left(m_{g_e}, \frac{m_{g_e} x}{d_{g_e}^{-\beta} \eta_1 \psi_e \lambda_{g_e}}\right).
 \tag{45}$$

From (45) into (44), and base on (42), Z_2^d can be formulated as

$$\begin{aligned}
 Z_2^d &= \frac{1}{\Gamma(m_{g_e}) \ln(2)} \int_0^\infty \frac{\Gamma\left(m_{g_e}, \frac{m_{g_e} x}{d_{g_e}^{-\beta} \eta_1 \psi_e \lambda_{g_e}}\right)}{1+x} dx \\
 &= \frac{1}{\Gamma(m_{g_e}) \ln(2)} \int_0^\infty \frac{G_{1,2}^{2,0}\left(1 \mid m_{g_e}, 0 \mid \frac{m_{g_e} x}{d_{g_e}^{-\beta} \eta_1 \psi_e \lambda_{g_e}}\right)}{1+x} dx.
 \end{aligned}
 \tag{46}$$

Similar to (43), with the aid of the [47, Eq. (7.811.5)], Z_2^d can be written by

$$Z_2^d = \frac{1}{\Gamma(m_{ge}) \ln(2)} G_{2,3}^{3,1} \left(\begin{matrix} 0, 1 \\ 0, m_{ge}, 0 \end{matrix} \middle| \frac{m_{ge}}{d_{ge}^{-\beta} \eta_1 \psi_e \lambda_{ge}} \right). \tag{47}$$

We can obtain (28) by converting (43) and (47) into (27).

Appendix B

From (29), W_1^d can be written by

$$W_1^d = \frac{1}{\ln 2} \int_0^\infty \frac{1 - F_{\gamma_{D_2}^{d,2}}(x)}{1+x} dx. \tag{48}$$

According to (17) and (23), $F_{\gamma_{D_2}^{d,2}}(x)$ can be given by

$$F_{\gamma_{D_2}^{d,2}}(x) = 1 - e^{-\frac{\lambda_d}{2}} \times \sum_{j=0}^\infty \frac{\lambda_d^j \Gamma(j+1/2, \frac{xN(1-\omega_d)}{2(\eta_2-x\eta_1)d_1^{-\beta}d_2^{-\beta}\psi\alpha^2})}{j!2^j\Gamma(j+1/2)}. \tag{49}$$

From (49) into (48), and W_1^d has to meet the requirement that $x < \frac{\eta_2}{\eta_1}$. So, W_1^d can be expressed as

$$W_1^d = \frac{1}{\ln 2} e^{-\frac{\lambda_d}{2}} \times \int_0^{\frac{\eta_2}{\eta_1}} \sum_{j=0}^\infty \frac{\lambda_d^j \Gamma(j+1/2, \frac{xN(1-\omega_d)}{2(\eta_2-x\eta_1)d_1^{-\beta}d_2^{-\beta}\psi\alpha^2})}{j!2^j\Gamma(j+1/2)(1+x)} dx. \tag{50}$$

Applying Gaussian–Chebyshev quadrature [47], W_1^d is given by

$$W_1^d = \frac{\pi \eta_2}{2\eta_1 K \ln 2} e^{-\frac{\lambda_d}{2}} \times \sum_{j=0}^\infty \sum_{k=1}^K \frac{\sqrt{1-t_k^2} \lambda_d^j \Gamma(j+1/2, \frac{\Theta N(1-\omega_d)}{2(\eta_2-\Theta\eta_1)d_1^{-\beta}d_2^{-\beta}\psi\alpha^2})}{j!2^j\Gamma(j+1/2)(1+\Theta)}, \tag{51}$$

where $\Theta = \frac{\eta_2 t_k + \eta_1}{2\eta_1}$, $t_k = \cos[\frac{(2k-1)\pi}{2K}]$.

Similarly, Z_2^d, W_2^d can be written as

$$W_2^d = \frac{1}{\Gamma(m_{ge}) \ln(2)} G_{2,3}^{3,1} \left(\begin{matrix} 0, 1 \\ 0, m_{ge}, 0 \end{matrix} \middle| \frac{m_{ge}}{d_{ge}^{-\beta} \eta_2 \psi_e \lambda_{ge}} \right). \tag{52}$$

We can obtain (30) by converting (51) and (52) into (29).

Appendix C

From (31), $COP_{D_1}^u$ can be given by (53), as shown at the top of the next page, where

$$\theta_1 = \frac{\gamma_{th1}}{d_g^{-\beta} \eta_1 \psi_1}, \theta_2 = \frac{d_1^{-\beta} d_2^{-\beta} \eta_2 \psi_2 \alpha^2}{N(1-\omega_u)}$$

$$\begin{aligned} COP_{D_1}^u &= 1 - \Pr \left(\frac{d_g^{-\beta} \eta_1 \psi_1 |g_u|^2}{d_1^{-\beta} d_2^{-\beta} \eta_2 \psi_2 \alpha^2 \frac{\left(\sum_{n=1}^N |h_{1,n}^u| |h_{2,n}^u|\right)^2}{N(1-\omega_u)} + 1} > \gamma_{th1} \right) \\ &= 1 - \Pr \left(|g_u|^2 > \frac{\gamma_{th1}}{d_g^{-\beta} \eta_1 \psi_1} \left(d_1^{-\beta} d_2^{-\beta} \eta_2 \psi_2 \alpha^2 \frac{\left(\sum_{n=1}^N |h_{1,n}^u| |h_{2,n}^u|\right)^2}{N(1-\omega_u)} + 1 \right) \right) \\ &= 1 - \Pr \left(|g_u|^2 > \theta_1 \left(\theta_2 \left(\sum_{n=1}^N |h_{1,n}^u| |h_{2,n}^u| \right)^2 + 1 \right) \right). \end{aligned} \tag{53}$$

Next, the CDF function of $|g_u|^2$ and the PDF of $\left(\sum_{n=1}^N |h_{1,n}^u| |h_{2,n}^u|\right)^2$ are given by (14) and (16), respectively. $COP_{D_1}^u$ can be derived as (54), as shown at the top of the next page, where $\delta = \frac{m_{gu} \theta_1 \theta_2}{\lambda_{gu}}$.

$$\begin{aligned} COP_{D_1}^u &= 1 - \int_0^\infty \left(1 - F_{|g_u|^2}(\theta_1(\theta_2 x + 1)) \right) f_{\left(\sum_{n=1}^N |h_{1,n}^u| |h_{2,n}^u|\right)^2}(x) dx \\ &= 1 - \int_0^\infty e^{-\frac{m_{gu} \theta_1 (\theta_2 x + 1)}{\lambda_{gu}}} \sum_{k=0}^{m_{gu}-1} \frac{1}{k!} \left(\frac{m_{gu} \theta_1 (\theta_2 x + 1)}{\lambda_{gu}} \right)^k e^{-\frac{x+\lambda_u}{2}} \sum_{j=0}^\infty \frac{\lambda_u^j x^{j-1/2}}{j! 2^{j+1/2} \Gamma(j+1/2)} dx \\ &= 1 - e^{-\frac{m_{gu} \theta_1}{\lambda_{gu}} - \frac{\lambda_u}{2}} \sum_{k=0}^{m_{gu}-1} \sum_{j=0}^\infty \int_0^\infty \frac{\lambda_u^j x^{j-1/2}}{k! j! 2^{j+1/2} \Gamma(j+1/2)} \left(\frac{m_{gu} \theta_1 (\theta_2 x + 1)}{\lambda_{gu}} \right)^k e^{-(\delta + \frac{1}{2})x} dx. \end{aligned} \tag{54}$$

Then, using the [47, Eq. (1.111)], $COP_{D_1}^u$ may be written by

$$\begin{aligned} COP_{D_1}^u &= 1 - e^{-\frac{m_{gu} \theta_1}{\lambda_{gu}} - \frac{\lambda_u}{2}} \sum_{k=0}^{m_{gu}-1} \sum_{j=0}^\infty \sum_{q=0}^k \binom{k}{q} \left(\frac{1}{\theta_2} \right)^{k-q} \\ &\quad \times \frac{\delta^k \lambda^j \Gamma(j+q+1/2)}{k! j! 2^{j+1/2} \Gamma(j+1/2)} \int_0^\infty x^{j+q+1/2-1} e^{-(\delta + \frac{1}{2})x} dx. \end{aligned} \tag{55}$$

The equation (32) can be attained from (55) with the aid of the [47, Eq. (3.381.4)].

Appendix D

Like (39) and (35), Z_1^u can be written by

$$Z_1^u = \frac{1}{\ln 2} \int_0^\infty \frac{1 - F_{\gamma_{D_1}^u}(x)}{1 + x} dx. \tag{56}$$

According to (32), the formula for $F_{\gamma_{D_1}^u}(x)$ is as follows

$$F_{\gamma_{D_1}^u}(x) = 1 - e^{-\frac{\lambda u}{2}} \sum_{k=0}^{m_{gu}-1} \sum_{j=0}^\infty \sum_{q=0}^k \binom{k}{q} \left(\frac{1}{\theta_2}\right)^{k-q} \times \frac{\lambda^j \Gamma(j + q + 1/2)}{k! j! 2^{2j+1/2} \Gamma(j + 1/2)} \times \left(\phi \theta_2 x + \frac{1}{2}\right)^{-(j+q+1/2)} (\phi \theta_2 x)^k e^{-\phi x}, \tag{57}$$

where $\phi = \frac{m_{gu}}{d_g^{-\beta} \eta_1 \psi_1 \lambda_{gu}}$.

As seen at the top of the following page, (58) can provide Z_1^u from (57) into (56).

$$Z_1^u = \frac{1}{\ln(2)} e^{-\frac{\lambda u}{2}} \sum_{k=0}^{m_{gu}-1} \sum_{j=0}^\infty \sum_{q=0}^k \binom{k}{q} \left(\frac{1}{\theta_2}\right)^{k-q} \left(\frac{1}{2}\right)^{-(j+q+1/2)} \frac{(\phi \theta_2)^k \lambda_u^j \Gamma(j + q + 1/2)}{k! j! 2^{2j+1/2} \Gamma(j + 1/2)} \times \int_0^\infty \frac{x^k e^{-\phi x}}{1 + x} (2\phi \theta_2 x + 1)^{-(j+q+1/2)} dx \tag{58}$$

$$= \frac{1}{\ln(2)} e^{-\frac{\lambda u}{2}} \sum_{k=0}^{m_{gu}-1} \sum_{j=0}^\infty \sum_{q=0}^k \binom{k}{q} \left(\frac{1}{\theta_2}\right)^{k-q} \left(\frac{1}{2}\right)^{-(j+q+1/2)} \frac{(\phi \theta_2)^k \lambda_u^j}{k! j! 2^{2j+1/2} \Gamma(j + 1/2)} \times \int_0^\infty x^{k+1-1} G_{0,1}^{1,0} \left(\phi x \middle| \begin{matrix} - \\ 0 \end{matrix} \right) G_{1,1}^{1,1} \left(x \middle| \begin{matrix} 0 \\ 0 \end{matrix} \right) G_{1,1}^{1,1} \left(2\phi \theta_2 x \middle| \begin{matrix} 1 - (j + q + 1/2) \\ 0 \end{matrix} \right) dx.$$

We employ the equalities [48, Eq. (2.6)] in (58) as

$$\frac{1}{1 + x} = G_{1,1}^{1,1} \left(x \middle| \begin{matrix} 0 \\ 0 \end{matrix} \right), \tag{59}$$

$$e^{-Ax} = G_{0,1}^{1,0} \left(Ax \middle| \begin{matrix} - \\ 0 \end{matrix} \right), \tag{60}$$

$$(Ax + 1)^{-B} = \frac{1}{\Gamma(B)} G_{1,1}^{1,1} \left(Ax \middle| \begin{matrix} 1 - B \\ 0 \end{matrix} \right). \tag{61}$$

From (58), with the help of the [49, Eq. (2.3)], Z_1^u can be written by (62), as shown at the top of the next page, where $H[\cdot, \dots, \cdot]$ is the multivariable Fox's H-function whose definition in terms of multiple Mellin–Barnes type contour integral is given in [48].

$$Z_1^u = \frac{1}{\ln(2)} e^{-\frac{\lambda u}{2}} \sum_{k=0}^{m_{gu}-1} \sum_{j=0}^\infty \sum_{q=0}^k \binom{k}{q} \left(\frac{1}{\theta_2}\right)^{k-q} \left(\frac{1}{2}\right)^{-(j+q+1/2)} \frac{(\phi \theta_2)^k \lambda_u^j \phi^{-k-1}}{k! j! 2^{2j+1/2} \Gamma(j + 1/2)} \times H_{1,0:1,1:1,1}^{0,1:1,1:1,1} \left(\begin{matrix} (-k, 1, 1) \\ - \end{matrix} \middle| \begin{matrix} (0, 1) \\ (0, 1) \end{matrix} \middle| \begin{matrix} (1 - (j + q + 1/2), 1) \\ (0, 1) \end{matrix} \middle| \frac{1}{\phi}, 2\theta_2 \right). \tag{62}$$

From (35) and similar (44), Z_2^u can be written by

$$Z_2^u = \frac{1}{\ln 2} \int_0^\infty \frac{1 - F_{\gamma_E^{u,1}}(x)}{1 + x} dx. \tag{63}$$

The formula for calculating $F_{\gamma_E^{u,1}}(x)$ using (14) and (34) is as follows

$$F_{\gamma_E^{u,1}}(x) = 1 - \frac{1}{\Gamma(m_{g_{e1}})} \Gamma\left(m_{g_{e1}}, \frac{m_{g_{e1}} x}{d_{g_{e1}}^{-\beta} \eta_1 \psi_{e1} \lambda_{g_{e1}}}\right). \tag{64}$$

Based on (42) and (64) into (63), Z_2^u can give by

$$\begin{aligned} Z_2^u &= \frac{1}{\Gamma(m_{g_{e1}}) \ln(2)} \int_0^\infty \frac{\Gamma\left(m_{g_{e1}}, \frac{m_{g_{e1}} x}{d_{g_{e1}}^{-\beta} \eta_1 \psi_{e1} \lambda_{g_{e1}}}\right)}{1 + x} dx \\ &= \frac{1}{\Gamma(m_{g_{e1}}) \ln(2)} \int_0^\infty \frac{G_{1,2}^{2,0}\left(1 \mid \frac{m_{g_{e1}} x}{d_{g_{e1}}^{-\beta} \eta_1 \psi_{e1} \lambda_{g_{e1}}}\right)}{1 + x} dx. \end{aligned} \tag{65}$$

In a manner similar (47), with the assistance of [47, Eq. (7.811.5)], Z_2^u can be written by

$$Z_2^u = \frac{1}{\Gamma(m_{g_{e1}}) \ln(2)} G_{2,3}^{3,1}\left(0, 1 \mid \frac{m_{g_{e1}}}{d_{g_{e1}}^{-\beta} \eta_1 \psi_{e1} \lambda_{g_{e1}}}\right). \tag{66}$$

We can obtain (36) by converting (62) and (66) into (35).

Appendix E

From (37) and similar to (48), W_1^u can be written by

$$W_1^u = \frac{1}{\ln 2} \int_0^\infty \frac{1 - F_{\gamma_{D_2}^u}(x)}{1 + x} dx. \tag{67}$$

Based on (33) $F_{\gamma_{D_2}^u}(x)$ can be calculated by

$$F_{\gamma_{D_2}^u}(x) = 1 - e^{-\frac{\lambda_u}{2}} \sum_{j=0}^\infty \frac{\lambda_u^j \Gamma\left(j + 1/2, \frac{x}{2\theta_2}\right)}{j! 2^j \Gamma(j + 1/2)}. \tag{68}$$

Based on (42) and (68) into (67), W_1^u can give by

$$\begin{aligned} W_1^u &= \frac{1}{\ln 2} e^{-\frac{\lambda_u}{2}} \sum_{j=0}^\infty \frac{\lambda_u^j}{j! 2^j \Gamma(j + 1/2)} \\ &\quad \times \int_0^\infty \frac{\Gamma\left(j + 1/2, \frac{x}{2\theta_2}\right)}{1 + x} dx \\ &= \frac{1}{\ln 2} e^{-\frac{\lambda_u}{2}} \sum_{j=0}^\infty \frac{\lambda_u^j}{j! 2^j \Gamma(j + 1/2)} \\ &\quad \times \int_0^\infty (x + 1)^{-1} G_{1,2}^{2,0}\left(0, j + 1/2 \mid \frac{x}{2\theta_2}\right) dx. \end{aligned} \tag{69}$$

Similar to (47), with the assistance of the [47, Eq. (7.811.5)], W_1^u can be written by

$$W_1^u = \frac{1}{\ln 2} e^{-\frac{\lambda_u}{2}} \sum_{j=0}^{\infty} \frac{\lambda_u^j}{j! 2^j \Gamma(j + 1/2)} \times G_{2,3}^{3,1} \left(\begin{matrix} 0, 1 \\ 0, 0, j + 1/2 \end{matrix} \middle| \frac{1}{2\theta_2} \right). \tag{70}$$

Similar to Z_2^u , W_2^u can write as

$$W_2^u = \frac{1}{\Gamma(m_{ge2}) \ln(2)} G_{2,3}^{3,1} \left(\begin{matrix} 0, 1 \\ 0, m_{ge2}, 0 \end{matrix} \middle| \frac{m_{ge2}}{d_{ge2}^{-\beta} \eta_2 \psi e^2 \lambda_{ge2}} \right). \tag{71}$$

From (70) and (71) into (37), we're able to get (38).

Abbreviations

IRS	Intelligent reflecting surface
RIS	Reflecting intelligent surface
LIS	Large intelligent surface
SE	Spectrum efficiency
EE	Energy efficiency
TDMA	Time division multiple access
FDMA	Frequency division multiple access
CDMA	Code division multiple access
NOMA	Non-orthogonal multiple access
OMA	Orthogonal multiple access
MA	Multiple access
SC	Superposition coding
PD	Power domain
SIC	Successive interference cancellation
IoT	Internet of thing
PLS	Physical layer security
COP	Connection outage probability
SOP	Secrecy outage probability
ASR	Average secrecy rate
BS	Base station
AWGN	Additive white Gaussian noises
SINR	Signal-to-interference-plus-noise ratio
SNR	Signal-to-noise ratio
PIC	Parallel interference cancelation
CLT	Central limit theorem
PDF	Probability density function
CDF	Cumulative distribution function

Acknowledgements

Not applicable.

Author contributions

All authors equally contributed to the work. All authors read and approved the final manuscript.

Funding

The research was co-funded by the European Union within the REFRESH project - Research Excellence For REgion Sustainability and High-tech Industries ID No. CZ.10.03.01/00/22_003/0000048 of the European Just Transition Fund and by the Ministry of Education, Youth and Sports of the Czech Republic (MEYS CZ) through the e-INFRA CZ project (ID:90254) and also by the MEYS CZ within the project SGS ID No. SP 7/2023 conducted by VSB-Technical University of Ostrava.

Availability of data and materials

Please contact the corresponding author for data requests.

Declarations

Competing Interests

The authors declare that they have no competing interests.

Received: 4 April 2023 Accepted: 23 September 2023

Published online: 11 October 2023

References

- Z. Zhang, Y. Xiao, Z. Ma, M. Xiao, Z. Ding, X. Lei, G.K. Karagiannidis, P. Fan, 6g wireless networks: vision, requirements, architecture, and key technologies. *IEEE Veh. Technol. Mag.* **14**(3), 28–41 (2019). <https://doi.org/10.1109/MVT.2019.2921208>
- M. Di Renzo, A. Zappone, M. Debbah, M.-S. Alouini, C. Yuen, J. de Rosny, S. Tretyakov, Smart radio environments empowered by reconfigurable intelligent surfaces: How it works, state of research, and the road ahead. *IEEE J. Sel. Areas Commun.* **38**(11), 2450–2525 (2020). <https://doi.org/10.1109/JSAC.2020.3007211>
- C. Liaskos, S. Nie, A. Tsiolaridou, A. Pitsillides, S. Ioannidis, I. Akyildiz, End-to-end wireless path deployment with intelligent surfaces using interpretable neural networks. *IEEE Trans. Commun.* **68**(11), 6792–6806 (2020). <https://doi.org/10.1109/TCOMM.2020.3012577>
- E. Basar, M. Di Renzo, J. De Rosny, M. Debbah, M.-S. Alouini, R. Zhang, Wireless communications through reconfigurable intelligent surfaces. *IEEE Access* **7**, 116753–116773 (2019). <https://doi.org/10.1109/ACCESS.2019.2935192>
- M.H. Dinan, N.S. Perović, M.F. Flanagan, RIS-assisted receive quadrature space-shift keying: a new paradigm and performance analysis. *IEEE Trans. Commun.* **70**(10), 6874–6889 (2022). <https://doi.org/10.1109/TCOMM.2022.3198117>
- M. Jung, W. Saad, Y. Jang, G. Kong, S. Choi, Reliability analysis of large intelligent surfaces (liss): rate distribution and outage probability. *IEEE Wirel. Commun. Lett.* **8**(6), 1662–1666 (2019). <https://doi.org/10.1109/LWC.2019.2935190>
- S. Hu, F. Rusek, O. Edfors, Beyond massive mimo: the potential of data transmission with large intelligent surfaces. *IEEE Trans. Signal Process.* **66**(10), 2746–2758 (2018). <https://doi.org/10.1109/TSP.2018.2816577>
- I. Yildirim, A. Uyrus, E. Basar, Modeling and analysis of reconfigurable intelligent surfaces for indoor and outdoor applications in future wireless networks. *IEEE Trans. Commun.* **69**(2), 1290–1301 (2021). <https://doi.org/10.1109/TCOMM.2020.3035391>
- B.C. Nguyen, T. Manh Hoang, A.-T. Le, V.D. Nguyen, P.T. Tran, Performance analysis of intelligent reflecting surface aided full-duplex amplify-and-forward relay networks. *Int. J. Commun. Syst.* **35**(10), 5172 (2022)
- N.D. Nguyen, A.-T. Le, M. Munochiveyi, F. Afghah, E. Pallis, Intelligent reflecting surface aided wireless systems with imperfect hardware. *Electronics* **11**(6), 900 (2022)
- L. Dai, B. Wang, Z. Ding, Z. Wang, S. Chen, L. Hanzo, A survey of non-orthogonal multiple access for 5g. *IEEE Commun. Surv. Tutor.* **20**(3), 2294–2323 (2018). <https://doi.org/10.1109/COMST.2018.2835558>
- D.-T. Do, A.-T. Le, Noma based cognitive relaying: transceiver hardware impairments, relay selection policies and outage performance comparison. *Comput. Commun.* **146**, 144–154 (2019)
- D.-T. Do, A.-T. Le, B.M. Lee, Noma in cooperative underlay cognitive radio networks under imperfect sic. *IEEE Access* **8**, 86180–86195 (2020). <https://doi.org/10.1109/ACCESS.2020.2992660>
- D.-T. Do, A.-T. Le, Y. Liu, A. Jamalipour, User grouping and energy harvesting in uav-noma system with af/df relaying. *IEEE Trans. Veh. Technol.* **70**(11), 11855–11868 (2021). <https://doi.org/10.1109/TVT.2021.3116101>
- Y. Saito, A. Benjebbour, Y. Kishiyama, T. Nakamura, System-level performance evaluation of downlink non-orthogonal multiple access (noma). In: 2013 IEEE 24th Annual International Symposium on Personal, Indoor, and Mobile Radio Communications (PIMRC), pp. 611–615 (2013). <https://doi.org/10.1109/PIMRC.2013.6666209>
- S.M.R. Islam, N. Avazov, O.A. Dobre, K.-s. Kwak, Power-domain non-orthogonal multiple access (noma) in 5g systems: potentials and challenges. *IEEE Commun. Surv. Tutor.* **19**(2), 721–742 (2017). <https://doi.org/10.1109/COMST.2016.2621116>
- H. Qiu, S. Gao, G. Tu, S. Zong, Position information-based noma for downlink and uplink transmission in mobile scenarios. *IEEE Access* **8**, 150808–150822 (2020). <https://doi.org/10.1109/ACCESS.2020.3017255>
- A.S.d. Sena, D. Carrillo, F. Fang, P.H.J. Nardelli, D.B.d. Costa, U.S. Dias, Z. Ding, C.B. Papadias, W. Saad, What role do intelligent reflecting surfaces play in multi-antenna non-orthogonal multiple access? *IEEE Wirel. Commun.* **27**(5), 24–31 (2020). <https://doi.org/10.1109/MWC.001.2000061>
- A.-T. Le, N.-D.X. Ha, D.-T. Do, A. Silva, S. Yadav, Enabling user grouping and fixed power allocation scheme for reconfigurable intelligent surfaces-aided wireless systems. *IEEE Access* **9**, 92263–92275 (2021). <https://doi.org/10.1109/ACCESS.2021.3092335>
- M. Munochiveyi, A.C. Pogaku, D.-T. Do, A.-T. Le, M. Voznak, N.D. Nguyen, Reconfigurable intelligent surface aided multi-user communications: state-of-the-art techniques and open issues. *IEEE Access* **9**, 118584–118605 (2021). <https://doi.org/10.1109/ACCESS.2021.3107316>
- A.-T. Le, D.-T. Do, H. Cao, S. Garg, G. Kaddoum, S. Mumtaz, Spectrum efficiency design for intelligent reflecting surface-aided iot systems. In: GLOBECOM 2022-2022 IEEE Global Communications Conference, pp. 25–30 (2022). <https://doi.org/10.1109/GLOBECOM48099.2022.10000937>
- Z. Ding, H. Vincent Poor, A simple design of irls-noma transmission. *IEEE Commun. Lett.* **24**(5), 1119–1123 (2020). <https://doi.org/10.1109/LCOMM.2020.2974196>
- F. Fang, Y. Xu, Q.-V. Pham, Z. Ding, Energy-efficient design of irls-noma networks. *IEEE Trans. Veh. Technol.* **69**(11), 14088–14092 (2020). <https://doi.org/10.1109/TVT.2020.3024005>
- X. Mu, Y. Liu, L. Guo, J. Lin, N. Al-Dhahir, Exploiting intelligent reflecting surfaces in noma networks: joint beamforming optimization. *IEEE Trans. Wirel. Commun.* **19**(10), 6884–6898 (2020). <https://doi.org/10.1109/TWC.2020.3006915>
- M. Fu, Y. Zhou, Y. Shi, Intelligent reflecting surface for downlink non-orthogonal multiple access networks. In: 2019 IEEE Globecom Workshops (GC Wkshps), pp. 1–6 (2019). <https://doi.org/10.1109/GCWkshps45667.2019.9024675>
- Y. Cheng, K.H. Li, Y. Liu, K.C. Teh, H. Vincent Poor, Downlink and uplink intelligent reflecting surface aided networks: noma and oma. *IEEE Trans. Wirel. Commun.* **20**(6), 3988–4000 (2021). <https://doi.org/10.1109/TWC.2021.3054841>

27. G. Yang, X. Xu, Y.-C. Liang, Intelligent reflecting surface assisted non-orthogonal multiple access. In: 2020 IEEE Wireless Communications and Networking Conference (WCNC), pp. 1–6 (2020). <https://doi.org/10.1109/WCNC45663.2020.9120476>
28. Z. Deng, Q. Li, Q. Zhang, L. Yang, J. Qin, Beamforming design for physical layer security in a two-way cognitive radio iot network with swipt. *IEEE Internet of Things J.* **6**(6), 10786–10798 (2019). <https://doi.org/10.1109/JIOT.2019.2941873>
29. D.-T. Do, A.-T. Le, N.-D.X. Ha, N.-N. Dao, Physical layer security for internet of things via reconfigurable intelligent surface. *Fut. Gener. Comput. Syst.* **126**, 330–339 (2022)
30. B. Schneier, Cryptographic design vulnerabilities. *Computer* **31**(9), 29–33 (1998)
31. A. Mukherjee, S.A.A. Fakoorian, J. Huang, A.L. Swindlehurst, Principles of physical layer security in multiuser wireless networks: a survey. *IEEE Commun. Surv. Tutor.* **16**(3), 1550–1573 (2014). <https://doi.org/10.1109/SURV.2014.012314.00178>
32. Z. Chu, W. Hao, P. Xiao, J. Shi, Intelligent reflecting surface aided multi-antenna secure transmission. *IEEE Wirel. Commun. Lett.* **9**(1), 108–112 (2020). <https://doi.org/10.1109/LWC.2019.2943559>
33. M. Cui, G. Zhang, R. Zhang, Secure wireless communication via intelligent reflecting surface. *IEEE Wirel. Commun. Lett.* **8**(5), 1410–1414 (2019). <https://doi.org/10.1109/LWC.2019.2919685>
34. L. Yang, J. Yang, W. Xie, M.O. Hasna, T. Tsiftsis, M.D. Renzo, Secrecy performance analysis of ris-aided wireless communication systems. *IEEE Trans. Veh. Technol.* **69**(10), 12296–12300 (2020). <https://doi.org/10.1109/TVT.2020.3007521>
35. X. Yu, D. Xu, R. Schober, Enabling secure wireless communications via intelligent reflecting surfaces. In: 2019 IEEE Global Communications Conference (GLOBECOM), pp. 1–6 (2019). <https://doi.org/10.1109/GLOBECOM38437.2019.9014322>
36. J. Chen, Y.-C. Liang, Y. Pei, H. Guo, Intelligent reflecting surface: a programmable wireless environment for physical layer security. *IEEE Access* **7**, 82599–82612 (2019). <https://doi.org/10.1109/ACCESS.2019.2924034>
37. J. Zuo, Y. Liu, E. Basar, O.A. Dobre, Intelligent reflecting surface enhanced millimeter-wave noma systems. *IEEE Commun. Lett.* **24**(11), 2632–2636 (2020). <https://doi.org/10.1109/LCOMM.2020.3009158>
38. X. Liu, Y. Liu, Y. Chen, H.V. Poor, Ris enhanced massive non-orthogonal multiple access networks: deployment and passive beamforming design. *IEEE J. Sel. Areas Commun.* **39**(4), 1057–1071 (2021). <https://doi.org/10.1109/JSAC.2020.3018823>
39. C. Gong, X. Yue, X. Wang, X. Dai, R. Zou, M. Essaaidi, Intelligent reflecting surface aided secure communications for noma networks. *IEEE Trans. Veh. Technol.* **71**(3), 2761–2773 (2022). <https://doi.org/10.1109/TVT.2021.3129075>
40. Z. Tang, T. Hou, Y. Liu, J. Zhang, L. Hanzo, Physical layer security of intelligent reflective surface aided noma networks. *IEEE Trans. Veh. Technol.* **71**(7), 7821–7834 (2022). <https://doi.org/10.1109/TVT.2022.3168392>
41. J. Chen, L. Yang, M.-S. Alouini, Physical layer security for cooperative noma systems. *IEEE Trans. Veh. Technol.* **67**(5), 4645–4649 (2018). <https://doi.org/10.1109/TVT.2017.2789223>
42. K. Cao, H. Ding, B. Wang, L. Lv, J. Tian, Q. Wei, F. Gong, Enhancing physical layer security for iot with non-orthogonal multiple access assisted semi-grant-free transmission. *IEEE Internet of Things J.* 1–1 (2022). <https://doi.org/10.1109/JIOT.2022.3193189>
43. J. Men, J. Ge, C. Zhang, Performance analysis of nonorthogonal multiple access for relaying networks over nakagami- m fading channels. *IEEE Trans. Veh. Technol.* **66**(2), 1200–1208 (2017). <https://doi.org/10.1109/TVT.2016.2555399>
44. Y. Song, W. Yang, Z. Xiang, B. Wang, Y. Cai, Secure transmission in mmwave noma networks with cognitive power allocation. *IEEE Access* **7**, 76104–76119 (2019). <https://doi.org/10.1109/ACCESS.2019.2920963>
45. X. Li, M. Zhao, M. Zeng, S. Mumtaz, V.G. Menon, Z. Ding, O.A. Dobre, Hardware impaired ambient backscatter noma systems: reliability and security. *IEEE Trans. Commun.* **69**(4), 2723–2736 (2021). <https://doi.org/10.1109/TCOMM.2021.3050503>
46. X. Liu, Average secrecy capacity of the weibull fading channel. In: 2016 13th IEEE Annual Consumer Communications & Networking Conference (CCNC), pp. 841–844 (2016). <https://doi.org/10.1109/CCNC.2016.7444897>
47. I.S. Gradshteyn, I.M. Ryzhik, Table of Integrals, Series, and Products. Academic press (2014)
48. A.M. Mathai, R.K. Saxena, H.J. Haubold, The H-function: Theory and Applications. Springer (2009)
49. P. Mittal, K. Gupta, An integral involving generalized function of two variables. In: Proceedings of the Indian Academy of Sciences-section A, vol. 75, pp. 117–123 (1972). Springer

Publisher's Note

Springer Nature remains neutral with regard to jurisdictional claims in published maps and institutional affiliations.